The Journal of Infectious Diseases

MAJOR ARTICLE

Shiga Toxin 2a–Induced Endothelial Injury in Hemolytic Uremic Syndrome: A Metabolomic Analysis

Christian Betzen,[1,2] Kathrin Plotnicki,[1] Farnoosh Fathalizadeh,[1] Kirk Pappan,[5] Thomas Fleming,[3] Martina Bielaszewska,[4] Helge Karch,[4] Burkhard Tönshoff,[1] and Neysan Rafat[1]

[1]Department of Pediatrics I, University Children's Hospital Heidelberg, [2]Division of Functional Genome Analysis, German Cancer Research Center, and [3]Department of Medicine I and Clinical Chemistry, University Hospital Heidelberg, and [4]Institute for Hygiene, University of Münster, Germany; and [5]Metabolon, Durham, North Carolina

Background. Endothelial dysfunction plays a pivotal role in the pathogenesis of postenteropathic hemolytic uremic syndrome (HUS), most commonly caused by Shiga toxin (Stx)–producing strains of *Escherichia coli*.

Methods. To identify new treatment targets, we performed a metabolomic high-throughput screening to analyze the effect of Stx2a, the major Stx type associated with HUS, on human renal glomerular endothelial cells (HRGEC) and umbilical vein endothelial cells (HUVEC). Cells were treated either with sensitizing tumor necrosis factor α (TNF-α) or Stx2a, a sequence of both or remained untreated.

Results. We identified 341 metabolites by combined liquid chromatography/tandem mass spectrometry and gas chromatography/mass spectrometry. Both cell lines exhibited distinct metabolic reaction profiles but shared elevated levels of free fatty acids. Stx2a predominantly altered the nicotinamide adenine dinucleotide (NAD) cofactor pathway and the inflammation-modulating eicosanoid pathway, which are associated with lipid metabolism. In HRGEC, Stx2a strongly diminished NAD derivatives, leading to depletion of the energy substrate acetyl coenzyme A and the antioxidant glutathione. HUVEC responded to TNF-α and Stx2a by increasing production of the counteracting eicosanoids prostaglandin I_2, E_1, E_2, and A_2, while in HRGEC only more prostaglandin I_2 was detected.

Conclusions. We conclude that disruption of energy metabolism and depletion of glutathione contributes to Stx-induced injury of the renal endothelium and that the inflammatory response to Stx is highly cell-type specific.

Keywords. hemolytic uremic syndrome; Shiga toxin; metabolomics; endothelial cells.

The postenteropathic hemolytic uremic syndrome (HUS) is the leading cause of acute renal failure in children beyond the neonatal period. Most of the cases are caused by infection with Shiga toxin (Stx)–producing strains of *Escherichia coli* (STEC). There is currently no specific treatment available for Stx-mediated HUS. The role of antimicrobial therapy has been discussed frequently in the past, but several studies identified antibiotic use as a significant risk factor for the subsequent development of HUS. This is because antibiotics increase the release of Stx from *E. coli*. Despite its sporadic occurrence, recent large-scale outbreaks, most notably the German 2011 epidemic [1], have demonstrated an urgent need for new approaches to HUS therapy development.

Stx-induced endothelial dysfunction, leading to thrombotic microangiopathy, plays a pivotal role in the pathogenesis of HUS [2–4]. Of the 2 major types of this toxin, Stx1a and Stx2a [5], the latter is most commonly associated with a clinical course of postenteropathic HUS [6, 7]. Stx particularly injures the microvascular beds of the gut, kidneys, and brain, causing bloody diarrhea, renal failure, and neurological complications [4, 8, 9].

Stx is a potent inhibitor of protein translation and acts on a broad range of cellular stress pathways [10], inducing proinflammatory, proapoptotic, and prothrombotic responses. To appreciate the complexity of interaction between Stx and the host cell, high-throughput so-called -omics methods offer both parallel assessment of multiple pathways and the chance of an unbiased discovery of new relevant cellular targets. For instance, proteomics and genomics approaches have quite recently been successfully used to better characterize the Stx-vector *E. coli* and have shed light on its interaction with the host environment [11]. Metabolomics provides an integrated view of cellular subsystems, as changes in genetic, epigenetic, posttranscriptional, and proteomic regulation all affect the metabolome of a cell. Alterations to this distinct biochemical signature indicate points of interaction between the host system and a drug or infectious agent, as already shown for Dengue virus [12]. In the present study, we therefore investigated the metabolic signature of Stx2a, in the presence or absence of presensitizing tumor necrosis factor α (TNF-α), in 2 human cell lines commonly used as an in vitro model of HUS, primary human renal glomerular

Received 30 July 2015; accepted 3 November 2015; published online 17 November 2015.

Presented in part: 4th International Conference on HUS-MPGN-TTP and Related Disorders, Innsbruck, Austria, 9–11 June 2013.

Correspondence: N. Rafat, Department of Pediatrics I, University Children's Hospital Heidelberg, 69120 Heidelberg, Germany (neysan.rafat@med.uni-heidelberg.de).

The Journal of Infectious Diseases® 2016;213:1031–40

DOI: 10.1093/infdis/jiv540

endothelial cells (HRGEC) and umbilical vein endothelial cells (HUVEC).

MATERIAL AND METHODS

For detailed Material and Methods, please see Supplementary Data.

Cell Culture and Treatments

We obtained HRGEC from ScienCell Research Laboratories (Carlsbad, California), and HUVEC were isolated from fresh umbilical cords or purchased commercially (Promocell, Heidelberg, Germany). Stx2a was purified as previously described [13]. The purified toxin was free of lipopolysaccharide, as determined with the Limulus assay (Bactimm, Nijmegen, the Netherlands; detection limit, 0.006 ng/mL); its protein concentration was 7.6 mg/mL, and its 50% cytotoxic dose for Vero cells was 0.072 ng/mL. TNF-α was acquired from Sigma (Deisenhofen, Germany). Preliminary dose-response experiments were performed on HUVEC and HRGEC to establish a minimal in vitro concentration needed to induce a full response to Stx (Supplementary Figure 1). HRGEC and HUVEC were treated with 1 μg/L TNF-α for 24 hours, with 1 μg/L Stx2a for 48 hours, or sequentially by prestimulation with TNF-α for 24 hours, followed by a change of medium and incubation with 1 μg/L Stx2a for an additional 48 hours. Unstimulated cells served as controls.

Sample Preparation for Metabolic Profiling

The metabolic profiling analysis combined 3 independent platforms: ultra–high-performance liquid chromatography/tandem mass spectrometry (UHPLC/MS-MS2) optimized for basic species, UHPLC/MS-MS2 optimized for acidic species, and gas chromatography/mass spectrometry (GC/MS). Samples were processed using the automated MicroLab STAR system (Hamilton Robotics, Reno, Nevada).

LC/MS

The LC/MS2 portion of the platform was based on a Waters ACQUITY UPLC (Waters, Milford, Massachusetts) and a Thermo-Finnigan LTQ mass spectrometer (San Jose, California), which consisted of an electrospray ionization source and a linear ion-trap mass analyzer. The MS analysis alternated between MS and data-dependent MS scans, using dynamic exclusion.

GC/MS

The samples destined for GC/MS analysis were redried under vacuum desiccation for a minimum of 24 hours prior to being derivatized under dried nitrogen, using bis trimethylsilyltriflouroacetamide. The GC column was 5% phenyl, and the temperature was ramped starting at 40°C. Derivatized samples for GC/MS were separated on a 5% diphenyl/95% dimethylpolysiloxane-fused silica column with helium as the carrier gas and a temperature ramp from 60°C to 340°C. Samples were then analyzed on a Thermo-Finnigan Trace DSQ MS (Thermo Fisher Scientific, Waltham, Massachusetts) operated at unit mass resolving power with electron impact ionization and a 50–750 atomic mass unit scan range (57).

Bioinformatics

Metabolites were identified by automated comparison of the ion features in the experimental samples to a reference library of chemical standard entries that included retention time, molecular weight (m/z), preferred adducts, and in-source fragments, as well as associated MS spectra, and were curated by visual inspection for quality control by using software developed at Metabolon (Durham, North Carolina).

Statistical Analysis

Missing values were assumed to be below the limits of detection, and these values were imputed with the compound minimum. Primary statistical analysis of log-transformed data was performed using R (available at: http://cran.r-project.org/). For agglomerative hierarchical clustering analysis, the fold change of each measured metabolite against the metabolite-specific median across all samples was calculated, and the resulting data set was submitted to complete-linkage hierarchical clustering with Pearson correlation distance. Further analyses were performed using Microsoft Excel (Microsoft; Redmond, Washington) and GraphPad Prism, version 6.00 for Windows (GraphPad Software, La Jolla, California), and the data set was transformed to ratios of treatment condition divided by mean of controls. Welch *t* tests and 2-way analysis of variance with the post hoc Dunnett correction for multiple testing were used to estimate the statistical significance of metabolite changes.

RESULTS

Global Metabolic Profile of HUVEC and HRGEC

A total of 341 different metabolites were identified across the spectrum of cellular biochemicals (Figure 1*A*). We performed agglomerative hierarchical clustering of metabolite changes to assess the global impact of treatment conditions on the metabolic profile. Irrespective of treatment, both cell lines could be clearly distinguished by hierarchical clustering and showed distinctive patterns of metabolite levels (Figure 1*B*). Only a minority of significant metabolic changes was shared between both cell lines (Figure 1*C*).

For most of the major metabolite groups and Stx2a-treatment conditions (Stx2a or TNF-α + Stx2a), we observed a net increase in detectable metabolite levels for both HUVEC and HRGEC (Figure 2). A significant increase in lipid levels was shared between HUVEC and HRGEC for all treatment conditions (TNF-α + Stx2a, 77.9% lipids of all shared, significantly changed metabolites; TNF-α, 42.9%; Stx2a, 42.9%; compared to 36.1% lipids in the overall metabolite set). A major fraction of these lipids consisted of free fatty acids (FFA).

Metabolite groups containing alterations by Stx2a or TNF-α + Stx2a were further analyzed according to inclusion of those metabolites in common pathways. We identified 2 major pathways

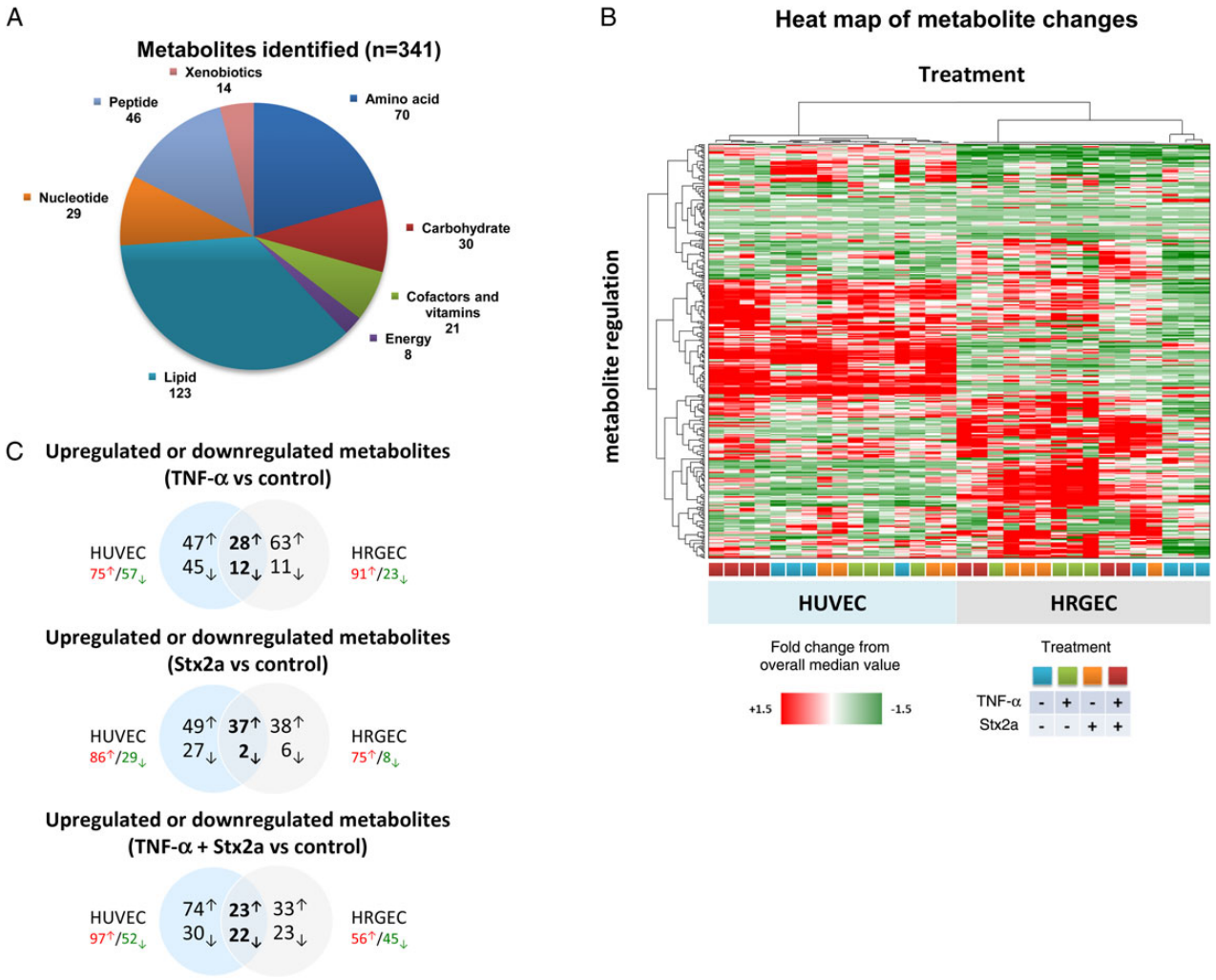

Figure 1. Global heatmap and summary of metabolites identified and significantly regulated in human umbilical vein endothelial cells (HUVEC) and renal glomerular endothelial cells (HRGEC) by tumor necrosis factor α (TNF-α), Shiga toxin 2a (Stx2a) or TNF-α + Stx2a. *A*, Breakdown of identified metabolites according to their biochemical nature. *B*, Heatmap of hierarchical clustering analysis, depicting fold change to overall median for all samples, treatment conditions and metabolites. In this type of graph, both conditions and metabolites that share the most similar metabolite patterns are sorted to be closest to each other. The hierarchal branching pattern further indicates the level of similarity, where the most dissimilar groups are split at the first branching. *C*, Summary of significantly ($P < .05$) increased or decreased metabolites for HUVEC or HRGEC. Intersects display number of metabolites with parallel changes in both cell lines. Cell specific totals are derived by adding the intersecting and non-intersecting numbers.

associated with lipid metabolism in which several clustered metabolite changes were mapped: (1) cellular energy metabolism linked to lipid-shuttling carnitine species, the nicotinamide adenine dinucleotide (NAD) cofactor pathway, and energy substrate acetyl coenzyme A (CoA); and (2) the inflammation-modulating eicosanoid pathway. Additional, yet more-ambiguous metabolic signatures of Stx were also found for carbohydrate (inhibition of glycolysis) and amino acid use (inhibition of mitochondrial oxidation of branched-chain amino acids and elevation of γ-glutamyl amino acid levels; Supplementary Figures 2–4 and Supplementary Tables 1–3).

Pathway Analysis: NAD/Lipid Energy Metabolism

In HUVEC, lipid-shuttling carnitine species responded with a minor net decrease after exposure to TNF-α alone but not to Stx2a alone or after sequential TNF-α + Stx2a treatment (Figure 3*A*). In HRGEC, a similar response to TNF-α was noticed. While Stx2a alone had no effect, sequential stimulation with TNF-α + Stx2a significantly decreased carnitine levels across all detectable species (Figure 3*B*).

Levels of acetyl CoA reflect the availability of lipid-derived substrates for cellular energy metabolism. HUVEC responded to lipid mobilization by increasing levels of acetyl CoA that were most pronounced after sequential stimulation with TNF-α + Stx2a (280.7% ± 85.2%) (Figure 4). On the other hand, HRGEC displayed strongly reduced levels of acetyl CoA when exposed to Stx2a and especially to TNF-α + Stx2a (<19.3% ± 6.1%), where levels of acetyl CoA dropped below the detection limit.

Several of the metabolites significantly altered by Stx2a or TNF-α + Stx2a in HRGEC were identified as members

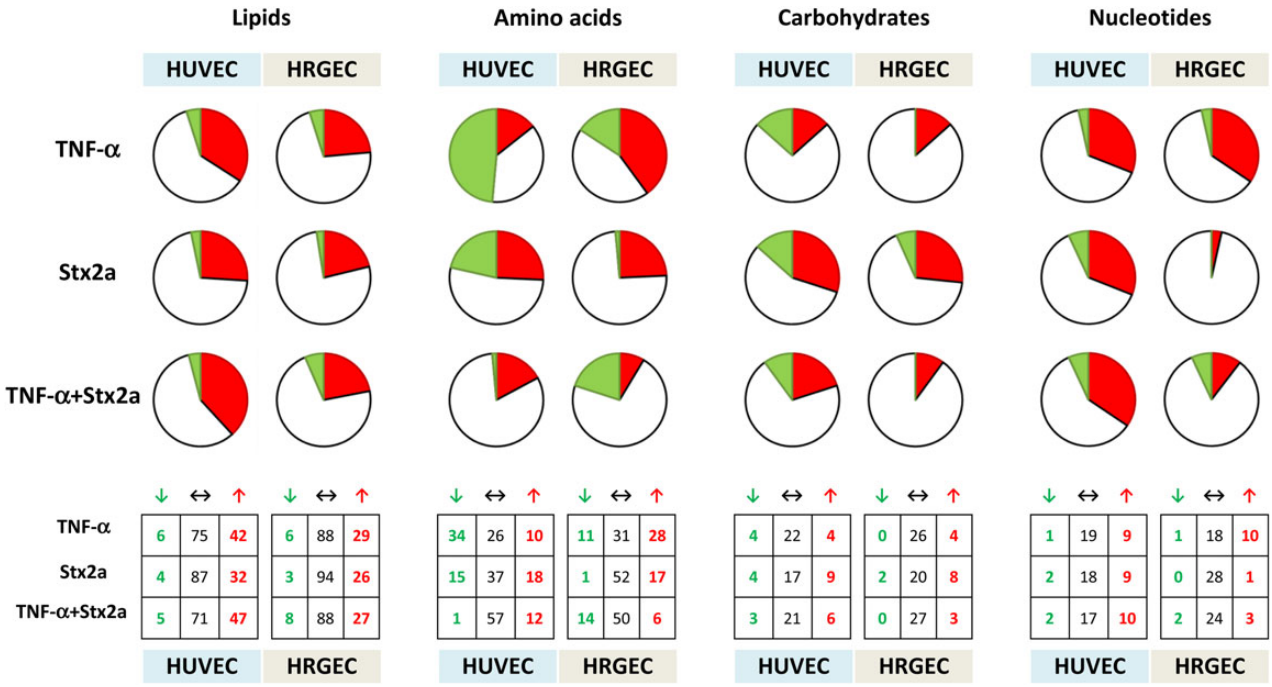

Figure 2. Changes in major metabolite groups (lipids, amino acids, carbohydrates and nucleotides) in response to tumor necrosis factor α (TNF-α), Shiga toxin 2a (Stx2a) or TNF-α + Stx2a in human umbilical vein endothelial cells (HUVEC) and renal glomerular endothelial cells (HRGEC). Pie charts display significantly ($P < .05$) increased (red) or decreased (green) metabolites in proportion to all metabolites of this group. Tables below summarize absolute numbers of significantly increased (red), decreased (green), or not significantly changed (black) metabolites per group. This figure is available in black and white in print and in color online.

of the NAD cofactor pathway (Figure 4 and Table 1). Both cell lines treated with TNF-α + Stx2a strongly accumulated kynurenine (HUVEC, 380.9% ± 54.0% [$P < .05$]; HRGEC, 3173.9% ± 1870.1% [$P < .01$]). In HRGEC, levels of NAD+ and derivative NADP were diminished after treatment with Stx2a (NAD+, 22.3% ± 20.1% [$P < .05$]; NADP, 12.3% ± 0.0% [$P < .01$]) or TNF-α + Stx2a (NAD+, 2.7% ± 1.0%; NADP, 12.3% ± 0.0% [$P < .01$]). Under the latter condition, NADH was reduced below the detection threshold. In HUVEC, only the NAD+ level was significantly reduced by treatment with TNF-α (69.6% ± 9.4%; $P < .01$) or TNF-α + Stx2a (61.6% ± 5.9%; $P < .01$) but not with Stx2a alone (98.8% ± 8.7%).

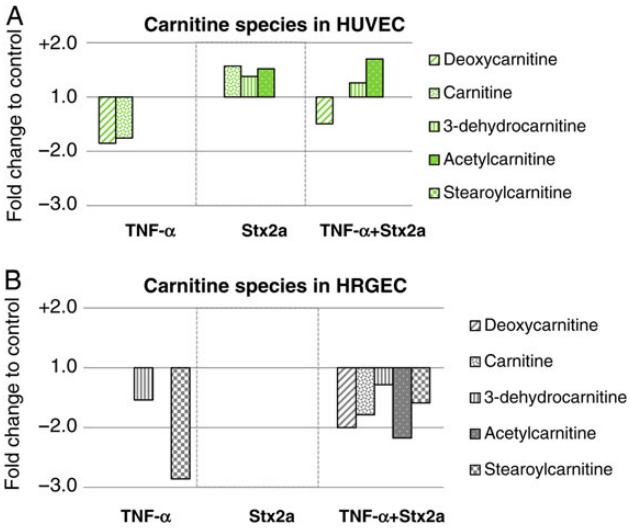

Figure 3. Levels of carnitine species in human umbilical vein endothelial cells (HUVEC; *A*) and renal glomerular endothelial cells (HRGEC; *B*) in response to tumor necrosis factor α (TNF-α), Shiga toxin 2a (Stx2a), or TNF-α + Stx2a. Bars indicate mean fold changes from control of significantly ($P < .05$) altered carnitine species in response to TNF-α, Stx2a, or TNF-α + Stx2a.

Pathway Analysis: Eicosanoid Pathway

Several key metabolites of inflammatory eicosanoid synthesis were significantly altered by Stx2a or TNF-α + Stx2a (Figure 5 and Table 2). HUVEC and HRGEC displayed different patterns of mediator generation. In HUVEC, treatment with TNF-α or TNF-α + Stx2a increased levels of both precursor linoleate and the early noninflammatory derivatives 13-HODE/9-HODE. In addition, a heterogeneous increase in levels of vasodilatory PGE_1 (TNF-α + Stx2a, 338.6% ± 90.5%; $P < .01$) and PGI_2 (represented by its stable breakdown product 6-keto-$PGF_{1\alpha}$), as well as the inflammation-modulating PGE_2 (TNF-α + Stx2a, 1038.2% ± 136.1%; $P < .01$) and PGA_2 (TNF-α + Stx2a, 1238.4% ±112.4%; $P < .01$), was noticed. Stimulation with Stx alone did not elicit significant changes, apart from an increase in 6-keto-$PGF_{1\alpha}$, (197.3% ± 22.9%; $P < .01$).

In HRGEC, TNF-α did not induce significant changes in eicosanoids. In contrast to HUVEC, the eicosanoid metabolism response to TNF-α + Stx2a in HRGEC was mostly

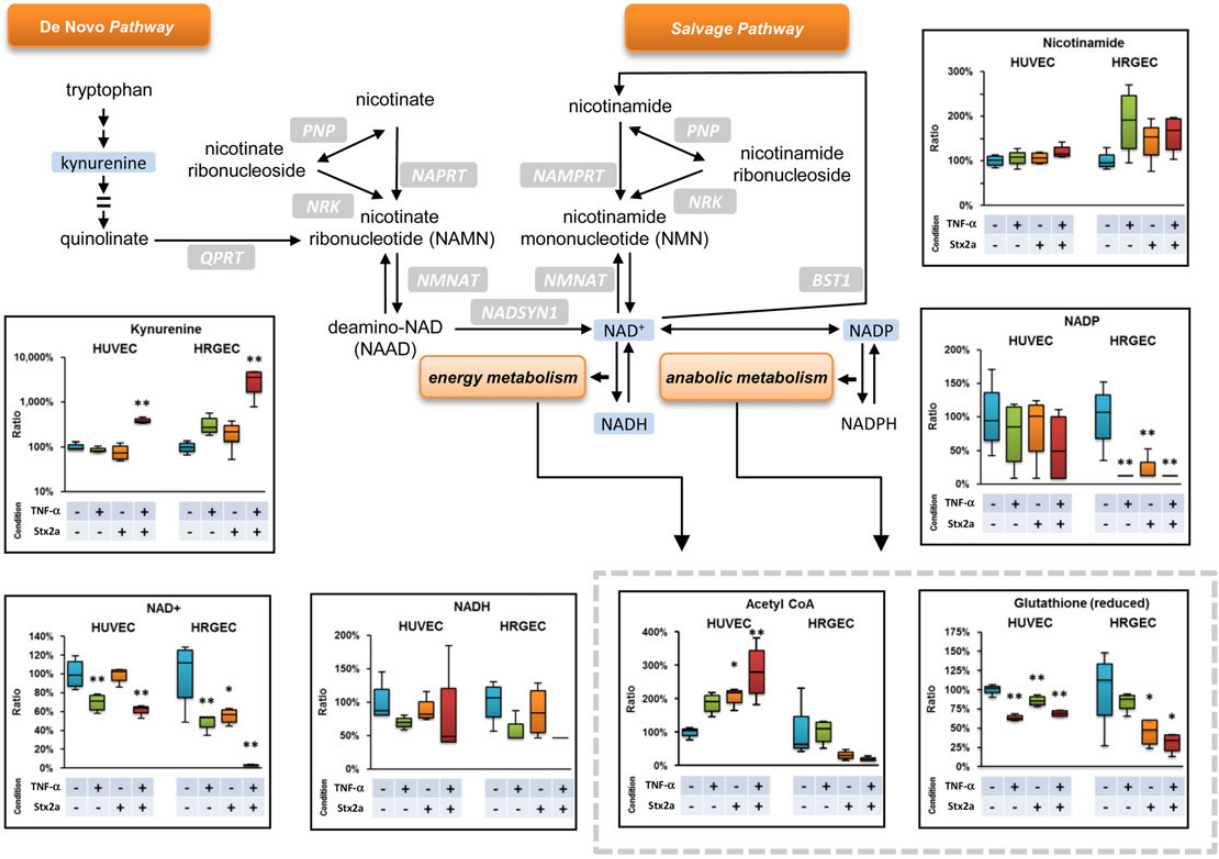

Figure 4. Shiga toxin 2a (Stx2a) reduces acetyl coenzyme A (CoA) and glutathione in human renal glomerular endothelial cells (HRGEC) via depletion of NAD cofactors. The simplified diagram depicts major reactions in the NAD de novo synthesis and salvage pathways. Metabolites detected and identified are highlighted in light blue, and enzymes are abbreviated and highlighted in gray. Insets show normalized levels of detected metabolites, summarized again in Table 1 as mean percentage (±SD) of control. Data are from 4 experiments. *$P < .05$ and **$P < .01$. Abbreviations: HUVEC, human umbilical vein endothelial cells; NAD, nicotinamide adenine dinucleotide. This figure is available in black and white in print and in color online.

Table 1. Shiga Toxin 2a (Stx2a) Reduces Acetyl Coenzyme A (CoA) and Glutathione Levels in Renal Glomerular Endothelial Cells (HRGEC) via Depletion of NAD Cofactors, by Treatment Condition

Cell Type, Metabolite	Control	TNF-α	Stx2a	TNF-α + Stx2a
HUVEC				
Acetyl CoA	100.0 ± 16.1	186.7 ± 31.7	206.7 ± 29.0[a]	280.7 ± 85.2[b]
Glutathione	100.0 ± 7.0	63.8 ± 3.8[b]	85.6 ± 6.8[b]	69.4 ± 4.0[b]
Kynurenine	100.0 ± 20.3	87.2 ± 12.5	80.0 ± 33.2	380.9 ± 54.0[b]
NAD+	100.0 ± 16.1	69.6 ± 9.4[b]	98.8 ± 8.7	61.6 ± 5.9[b]
NADH	100.0 ± 30.7	69.7 ± 9.0	88.3 ± 19.0	80.6 ± 69.8
NADP	100.0 ± 53.2	74.1 ± 51.0	83.1 ± 51.7	54.1 ± 53.4
Nicotinamide	100.0 ± 12.6	106.3 ± 19.3	106.0 ± 13.0	120.0 ± 15.4
HRGEC				
Acetyl CoA	100.0 ± 87.9	101.1 ± 37.2	31.4 ± 13.4	19.3 ± 6.1
Glutathione	100.0 ± 51.6	84.0 ± 12.7	44.9 ± 18.4[a]	30.7 ± 13.3[a]
Kynurenine	100.0 ± 28.9	318.1 ± 168.0	212.7 ± 128.5	3173.9 ± 1870.1[b]
NAD+	100.0 ± 36.1	48.9 ± 9.6[b]	55.2 ± 8.2[a]	2.7 ± 1.0[b]
NADH	100.0 ± 31.8	56.8 ± 20.3	85.9 ± 38.1	46.6 ± 0.0
NADP	100.0 ± 48.5	12.3 ± 0.0[b]	22.3 ± 20.1[b]	12.3 ± 0.0[b]
Nicotinamide	100.0 ± 20.8	186.4 ± 75.8	143.8 ± 49.3	159.2 ± 43.4

Data are mean % (±SD) of control for 4 experiments.

Abbreviations: HUVEC, human umbilical vein endothelial cells; NAD, nicotinamide adenine dinucleotide; TNF-α, tumor necrosis factor α.

[a] $P < .05$.

[b] $P < .01$.

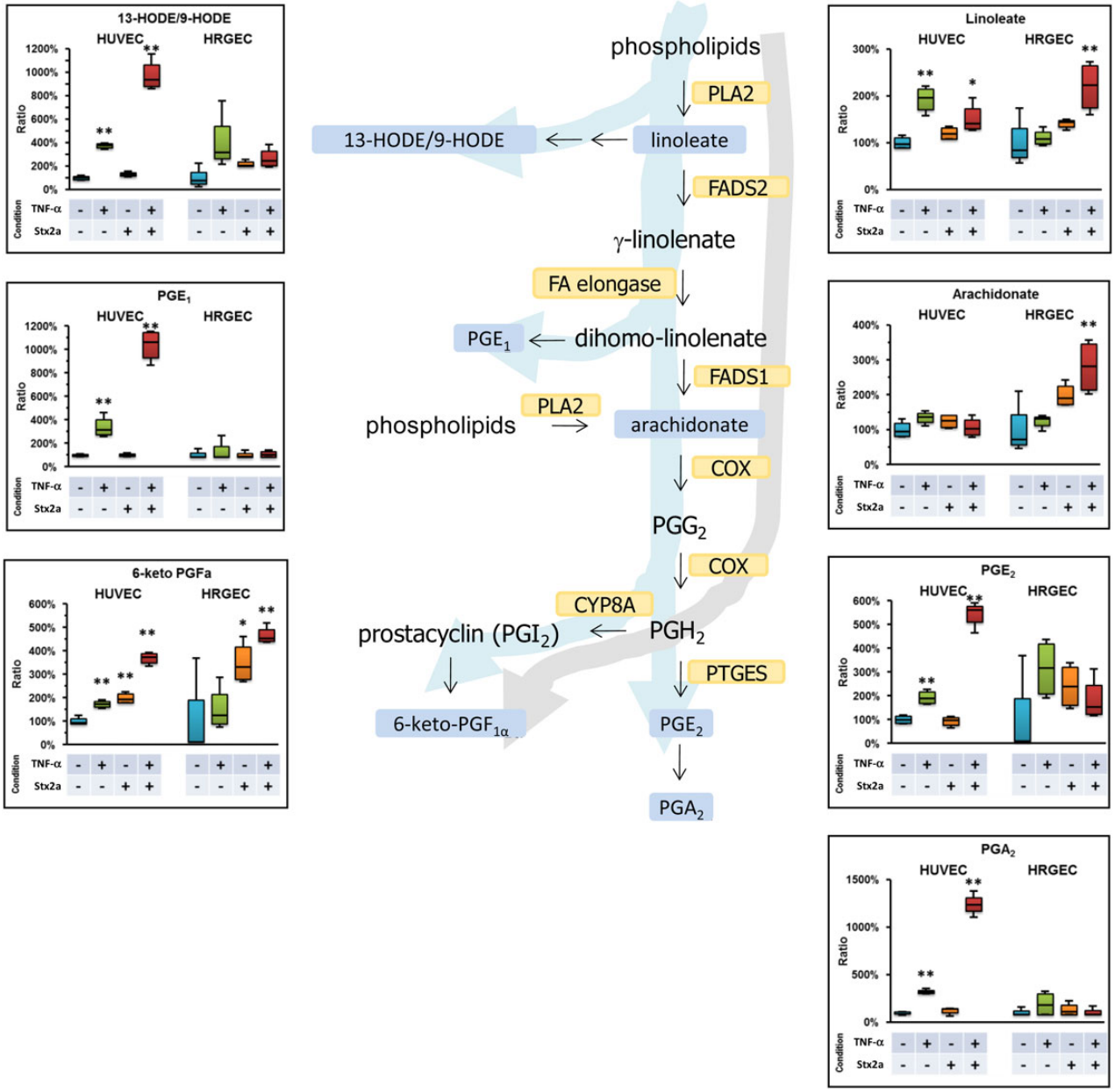

Figure 5. Shiga toxin (Stx) induces cell-line specific patterns of eicosanoid generation in human umbilical vein endothelial cells (HUVEC) and renal glomerular endothelial cells (HRGEC). The simplified diagram depicts major reactions in the eicosanoid synthesis pathway. Metabolites detected and identified are highlighted in light blue, enzymes abbreviated and highlighted in yellow. Insets: normalized levels of detected metabolites, summarized again in Table 2 below as mean percentage of control ±SD. *$P < .05$, **$P < .01$, and n = 4. Abbreviation: TNF-α, tumor necrosis factor α. This figure is available in black and white in print and in color online.

restricted to increases in the levels of PGI_2/6-keto-$PGF_{1\alpha}$ (Stx2a, 347.3% ±87.6% [$P < .05$]; TNF-α + Stx2a, 465.3 ± 37.4 [$P < .01$]), along with the precursors linoleate and arachidonic acid. HRGEC treated with Stx2a alone mirrored the response to TNF-α +Stx2a numerically but reached statistical significance only for 6-keto-$PGF_{1\alpha}$.

DISCUSSION

Here, we report the first study to investigate the global metabolomic profile of primary HRGEC and HUVEC in response to Stx2a, the major Stx type involved in the pathogenesis of post-enteropathic HUS [6, 7, 14, 15].

We observed that the global metabolomic profile under baseline conditions and in response to Stx2a strongly differed between HUVEC and HRGEC. Despite these differences, both cell lines shared elevated levels of lipids in response to treatment with Stx2a, especially of FFA. FFA may be released from cellular membranes as a byproduct of Stx-induced increased expression and activity of phospholipase PLA_2, promoting its retrograde transport [16]. FFA thus released may then be recruited as

Table 2. Shiga Toxin 2a (Stx2a) Induces Cell-Line–Specific Patterns of Eicosanoid Generation in Human Umbilical Vein Endothelial Cells (HUVEC) and Renal Glomerular Endothelial Cells (HRGEC), by Treatment Condition

Cell Type, Metabolite	Control	TNF-α	Stx2a	TNF-α + Stx2a
HUVEC				
13-/9-HODE	100.0 ± 17.5	373.8 ± 23.3[a]	130.7 ± 21.1	973.2 ± 131.4[a]
6-keto-$PGF_{1\alpha}$	100.0 ± 16.7	172.8 ± 15.4[a]	197.3 ± 22.9[a]	368.3 ± 26.1[a]
Arachidonate	100.0 ± 23.4	134.3 ± 18.2	123.8 ± 20.4	106.6 ± 27.3
Linoleate	100.0 ± 13.5	192.8 ± 28.3[a]	120.4 ± 14.1	151.4 ± 31.2[b]
PGA_2	100.0 ± 18.0	321.5 ± 22.8[a]	123.1 ± 38.3	1238.4 ± 112.4[a]
PGE_1	100.0 ± 9.7	338.6 ± 90.5[a]	101.2 ± 13.2	1038.2 ± 136.1[a]
PGE_2	100.0 ± 17.7	192.8 ± 28.7[a]	93.5 ± 21.3	544.3 ± 54.8[a]
HRGEC				
13-/9-HODE	100.0 ± 85.3	401.7 ± 241.4	218.4 ± 26.2	266.6 ± 85.9
6-keto-$PGF_{1\alpha}$	100.0 ± 179.9	151.7 ± 93.7	347.3 ± 87.6[b]	465.3 ± 37.4[a]
Arachidonate	100.0 ± 74.1	124.4 ± 19.7	198.5 ± 33.4	279.9 ± 76.8[a]
Linoleate	100.0 ± 51.0	110.9 ± 17.0	141.2 ± 10.0	219.9 ± 53.6[a]
PGA_2	100.0 ± 38.5	190.6 ± 128.6	131.6 ± 67.6	103.0 ± 44.6
PGE_1	100.0 ± 34.9	128.2 ± 91.4	99.0 ± 28.2	107.7 ± 29.5
PGE_2	100.0 ± 179.4	315.2 ± 123.2	241.3 ± 94.1	184.1 ± 90.3

Data are mean % (±SD) of control for 4 experiments.

Abbreviation: TNF-α, tumor necrosis factor α.

[a] $P < .01$.

[b] $P < .05$.

substrate for energy metabolism or provide the scaffold for lipid-derived mediators, such as eicosanoids. However, the metabolic signatures of carnitines, NAD derivatives, and acetyl CoA indicate that, in HRGEC treated with TNF-α + Stx2a, lipid energy metabolism is disrupted. Carnitine species facilitate the transmembrane transport of FFA to the mitochondrial compartment for beta-oxidation. Because of this crucial function, their levels are physiologically maintained within narrow limits and may therefore be used as surrogate markers of lipid metabolism activity [17]. Among the significantly regulated metabolites following treatment with TNF-α + Stx2a, levels of carnitines across all detected species were diminished in HRGEC, reflecting a perturbation of FFA use for energy metabolism.

Further disturbance of lipid metabolism may be caused by the Stx2a-induced depletion of the NAD cofactor family, NAD(H) and NADP(H). Adequate levels of NADH are essential for sustaining effective energy metabolism. In HRGEC, where NAD+ and NADH were severely depleted following treatment with Stx2a or TNF-α + Stx2a, acetyl CoA was concomitantly diminished down to detection threshold. In HUVEC, however, where the impact of Stx2a on NAD+ or NADH levels was less pronounced, the cellular acetyl CoA content even increased under these conditions. NADPH is required for regeneration of reduced glutathione (GSH). In the cell, GSH is the primary nonprotein radical scavenger protecting proteins, lipids, and DNA from oxidative damage by, for example, reactive oxygen species [18]. Oxidative stress and renal depletion of GSH play a role for in vivo models of HUS. In mice, Stx2 induces strong oxidative stress, exceeding the antioxidant capacity and depleting the renal GSH content. Treatment with GSH precursors 48 hours before or concomitant with Stx2 injection partially improved survival and blood parameters [19]. In humans, oxidative stress was reported in a study of 18 patients with STEC-HUS [20], and Stxs produce reactive oxygen species in vitro in human blood [21]. Indicators of oxidative stress could also be detected in our study: 9- and 13-HODE, derivatives of arachidonic acid, were elevated in both HUVEC and HRGEC. Levels of HODE are generally reported to be increased in oxidative environments and have been proposed as biomarkers of oxidative stress [22]. In HRGEC, depletion of NADP by Stx2a and TNF-α + Stx2a was mirrored by depletion of GSH, compromising cellular antioxidant capacity. In addition to GSH depletion, both cell lines had reduced levels of antioxidative sulfur-containing amino acids (data not shown).

Therefore, exhaustion of cellular GSH stores, either directly through increased production of reactive oxygen species or indirectly by means of NAD cofactor depletion, might expose Stx-sensitive cells to oxidative damage. Depletion of GSH is also a key event in early apoptosis, where GSH serves as a critical gatekeeper both in extrinsic and intrinsic apoptotic signaling cascades [23–25]. Of note, GSH depletion has been reported for other members of the bacterial A-B toxin family, ricin and cholera toxin. Ricin induces apoptosis by depleting cells of intracellular NAD+, ATP, and GSH [26, 27]. In one study, specific PARP inhibitor 3-aminobenzamide prevented NAD+ and ATP depletion and protected U937 cells from ricin-induced cytolysis [26]. Cholera toxin decreases GSH content of intestinal mucosa

in rats, although toxin-induced fluid secretion was not influenced by either depletion or supplementation of thiols [28].

On the basis of our findings, we conclude that the observed reduction in cellular NAD(P) and GSH content by Stx compromises both cellular energy metabolism and antioxidative and antiapoptotic capacity of HRGEC.

Levels of eicosanoid inflammatory mediators were strongly elevated in both HUVEC and HRGEC. This is in line with previous reports that Stx-exposed human cells mount an eicosanoid response. In the macrophage-like cell line THP-1, Stx1 increased PGE_2 and thromboxane levels in culture supernatant [29]. Similar results were obtained for isolated glomerular epithelial cells [30]. Yet, although both are of endothelial origin, the inflammatory signatures of Stx2a in HUVEC and HRGEC were quite different, as HRGEC increased only PGI_2 synthesis. HRGEC had previously been shown to release PGI_2 after Stx treatment [31]. Although macrovascular rat aortic rings were reported to reduce PGI_2 synthesis in response to Stxs [32], we found that macrovascular HUVEC displayed an increase in PGI_2 level in response to Stx similar to that seen in HRGEC. The clinical implications of PGI_2 levels in HUS are unclear. Children with HUS display an elevated PGI_2 plasma level [33–35] but a reduced 6-keto-$PGF_{1\alpha}$ level in urine during the acute phase [36]. Furthermore, in a baboon model of HUS, an increased PGI_2 level did not protect from death [37], and intravenous administration of PGI_2 in HUS has produced inconsistent results [38, 39]. The role of eicosanoids, especially PGI_2, in HUS therefore remains controversial [40, 41].

When looking at inflammatory mediators, both cell lines in our study treated with TNF-α + Stx2a strongly accumulated kynurenine. Activation of the kynurenine pathway has been associated with endothelial dysfunction and the progression of atherosclerosis in patients with chronic kidney disease [42]. Plasma kynurenine pathway metabolites accumulated in experimental chronic renal failure [43] and in patients with uremia [44] and have been associated with inflammation and infection [45], representing an early mediator of leukocyte recruitment to vascular endothelium [46]. Whether the accumulation of kynurenine is simply a nonspecific result of the proinflammatory stimulation by TNF-α and Stx2a or whether it has a specific pathogenic role in Stx-mediated HUS can only be speculated and needs further examination.

Of the published transcriptomics data mapping the regulation of up to 14 500 genes [16–19], only few genes (up to 369) were found to be affected by Stx. Most of the genes affected in these studies are involved in the regulation of chemokines, cytokines, and cellular adhesion molecules, as well as signaling molecules and transcription factors related to immune response and the induction of apoptosis. Only very few transcriptional targets (prostaglandin metabolism, PPARA, and SLC6A15) seem to be related to the control of cellular metabolism. This seeming discrepancy may in part be due to different experimental settings and approaches (ie, choice of cell lines, Stx type, and subinhibitory vs proapoptotic concentrations) but may also be related to metabolic regulatory signaling on a nontranscriptional level.

All 3 studies that have used high-throughput microarrays reported the upregulation of prostaglandins or related enzymes and receptors, supporting our observation that increased prostaglandin metabolism is a central feature of the host response to Stx.

One study reported induction of PPARA, a regulator of the peroxisomal β-oxidation pathway of fatty acids, whose plethora of transcriptional targets support the uptake, use, and catabolism of fatty acids [18]. PPARA is activated in cells deprived of energy or exposed to increased levels of fatty acid metabolites, such as arachidonic acid or derivatives of linoleic acid, with both conditions observed in our model. Therefore, PPARA upregulation as a cellular countermeasure fits well within our model of fatty acid metabolism disruption, energy depletion, and upregulation of prostaglandin metabolism by Stx.

SLC6A15 encodes a transporter for transporter for neutral, preferably branched-chain amino acids [18]. We did not, however, observe any relevant changes in the cellular levels of these amino acids in either of the cell lines studied.

Several caveats need to be addressed in the interpretation of our study. For most of the analyzed metabolites, the overall effect of the different treatment conditions remained subtle. Levels of only a few metabolites changed in excess of 2-fold above or below control, although some displayed dramatic changes, such as kynurenine. The focus of this study was on the intracellular metabolome, since we anticipated that intracellular metabolites would be most affected by Stx ± TNF-α, but in fact many of the most-affected metabolites are soluble or secreted factors. It would therefore be interesting to perform metabolomics on the supernatant from the cells, which will be the focus of future studies. Possibly, the changes found there are even more striking than those already reported.

Serum values for Stx2 have only been reported in 3 children in a large Argentinean cohort study, with the highest baseline levels ranging from 10.5 to 17.3 pg/mL [6], roughly corresponding to a hundredth of the dose used in our study (1 μg/L). However, since a peak value for Stx2 could not be established in any of these patients, the effective serum concentration of Stx2 necessary to initiate HUS in humans remains unclear. No other study so far has directly measured blood levels of Stx in time in HUS patients, most likely owing to the relatively late presentation of patients at the time of systemic disease onset and/or rapid sequestration of the toxin by an as yet unknown mechanism. In addition, it has been proposed that Stx targeting the endothelium might be bound to cellular carriers like polymorphonuclear leukocytes, thus potentially reaching much higher effective concentrations at the endothelial target site [7].

The dose of Stx2 used in our study lies well within the range used by other studies (0.068–3.4 μg/L) investigating the effects of Stx2 on human endothelial and tubular cell lines [9–13].

For some of the pathways investigated in our screening, stimulation with proinflammatory TNF-α alone induced metabolite response patterns similar to those induced by Stx2a or TNF-α + Stx2a. TNF-α renders HUVEC and HRGEC adequately responsive to in vitro Stx receptor upregulation [47] but may induce inflammatory responses and induce or block apoptosis in endothelial cells [48]. To reduce the potential influence of TNF-α on the metabolic profile, we opted for a low TNF-α concentration of 1 μg/L for prestimulation purposes, between the orders of magnitude reported in vivo (0.1 μg/L) [49] and those commonly used in vitro (10 μg/L) [50], and have found this level to adequately induce sensitivity for Stx in our investigated cells types. In the future, use of microvascular endothelial cell lines that constitutively express Stx receptor in the absence of prestimulating factors may improve specificity in investigating Stx-induced cell damage.

In conclusion, this is, to our knowledge, the first study to investigate the global impact of Stx2a on human host cell metabolism. We observed discrete but distinct patterns of metabolic response to Stx2a in HUVEC and HRGEC. Recruitment of fatty acids was shared by both cell lines. However, whereas in HUVEC this led to increases in energy rich acetyl CoA and a range of inflammatory eicosanoids (PGI_2, PGE_2, and PGA_2), use of FFA for oxidation in HRGEC was confounded by reduced availability of FFA-shuttling carnitines and dysregulation of NAD metabolism. Consequently, we observed depletion of cellular antioxidant capacity and exhaustion of acetyl CoA. In contrast to HUVEC, HRGEC channeled available eicosanoid precursors primarily into production of PGI_2. Stx2a-induced disruption of NAD-dependent energy metabolism and cellular glutathione levels could provide a new avenue for future investigation and a potential target for pharmacological modulation of Stx-related disease.

Supplementary Data

Supplementary materials are available at http://jid.oxfordjournals.org. Consisting of data provided by the author to benefit the reader, the posted materials are not copyedited and are the sole responsibility of the author, so questions or comments should be addressed to the author.

Notes

Acknowledgments. We thank Dr Jörg Hoheisel for a critical reading of the manuscript.

Financial support. This work was supported by the Medical Faculty of the University of Heidelberg (physician scientist fellowship grant to C. B. and N. R.).

Potential conflicts of interest. All authors: No reported conflicts. All authors have submitted the ICMJE Form for Disclosure of Potential Conflicts of Interest. Conflicts that the editors consider relevant to the content of the manuscript have been disclosed.

References

1. Robert Koch Institut. Final presentation and evaluation of epidemiological findings in the EHEC O104:H4 outbreak, Germany 2011. Berlin: Robert Koch Instiute, **2011**.
2. Proulx F, Seidman EG, Karpman D. Pathogenesis of Shiga toxin-associated hemolytic uremic syndrome. Pediatr Res **2001**; 50:163–71.
3. Tarr PI, Gordon CA, Chandler WL. Shiga-toxin-producing *Escherichia coli* and haemolytic uraemic syndrome. Lancet **2005**; 365:1073–86.
4. Karmali MA. Infection by Shiga toxin-producing *Escherichia coli*: an overview. Mol Biotechnol **2004**; 26:117–22.
5. Scheutz F, Teel LD, Beutin L, et al. Multicenter evaluation of a sequence-based protocol for subtyping shiga toxins and standardizing stx nomenclature. J Clin Microbiol **2012**; 50:2951–63.
6. Ostroff SM, Tarr PI, Neill MA, Lewis JH, Hargrett-Bean N, Kobayashi JM. Toxin genotypes and plasmid profiles as determinants of systemic sequelae in Escherichia coli O157:H7 infections. J Infect Dis **1989**; 160:994–8.
7. Friedrich AW, Bielaszewska M, Zhang W-L, et al. *Escherichia coli* harboring Shiga toxin 2 gene variants: frequency and association with clinical symptoms. J Infect Dis **2002**; 185:74–84.
8. Karch H, Tarr PI, Bielaszewska M. Enterohaemorrhagic *Escherichia coli* in human medicine. Int J Med Microbiol **2005**; 295:405–18.
9. Bielaszewska M, Karch H. Consequences of enterohaemorrhagic *Escherichia coli* infection for the vascular endothelium. Thromb Haemost **2005**; 94:312–8.
10. Tesh VL. Activation of cell stress response pathways by Shiga toxins. Cell Microbiol **2012**; 14:1–9.
11. Pieper R, Zhang Q, Clark DJ, et al. Proteomic view of interactions of Shiga toxin-producing *Escherichia coli* with the intestinal environment in gnotobiotic piglets. PLoS One **2013**; 8:e66462.
12. Birungi G, Chen SM, Loy BP, Ng ML, Li SFY. Metabolomics approach for investigation of effects of dengue virus infection using the EA.hy926 cell line. J Proteome Res **2010**; 9:6523–34.
13. Bauwens A, Bielaszewska M, Kemper B, et al. Differential cytotoxic actions of Shiga toxin 1 and Shiga toxin 2 on microvascular and macrovascular endothelial cells. Thromb Haemost **2011**; 105:515–28.
14. Hashimoto H, Mizukoshi K, Nishi M, et al. Epidemic of gastrointestinal tract infection including hemorrhagic colitis attributable to Shiga toxin 1-producing *Escherichia coli* O118:H2 at a junior high school in Japan. Pediatrics **1999**; 103:E2.
15. Scotland SM, Willshaw GA, Smith HR, Rowe B. Properties of strains of *Escherichia coli* belonging to serogroup O157 with special reference to production of Vero cytotoxins VT1 and VT2. Epidemiol Infect **1987**; 99:613–24.
16. Tcatchoff L, Andersson S, Utskarpen A, et al. Annexin A1 and A2: roles in retrograde trafficking of Shiga toxin. PLoS One **2012**; 7:e40429.
17. Reuter SE, Evans AM. Carnitine and acylcarnitines: pharmacokinetic, pharmacological and clinical aspects. Clin Pharmacokinet **2012**; 51:553–72.
18. Armstrong JS, Jones DP. Glutathione depletion enforces the mitochondrial permeability transition and causes cell death in Bcl-2 overexpressing HL60 cells. FASEB J **2002**; 16:1263–5.
19. Gomez SA, Abrey-Recalde MJ, Panek CA, et al. The oxidative stress induced in vivo by Shiga toxin-2 contributes to the pathogenicity of haemolytic uraemic syndrome. Clin Exp Immunol **2013**; 173:463–72.
20. Ferraris V, Acquier A, Ferraris JR, Vallejo G, Paz C, Mendez CF. Oxidative stress status during the acute phase of haemolytic uraemic syndrome. Nephrol Dial Transplant **2011**; 26:858–64.
21. Aiassa V, Baronetti JL, Paez PL, et al. Increased advanced oxidation of protein products and enhanced total antioxidant capacity in plasma by action of toxins of *Escherichia coli* STEC. Toxicol In Vitro **2011**; 25:426–31.
22. Niki E. Lipid peroxidation products as oxidative stress biomarkers. Biofactors **2008**; 34:171–80.
23. Brown GC, Borutaite V. Regulation of apoptosis by the redox state of cytochrome c. Biochim Biophys Acta **2008**; 1777:877–81.
24. Sato T, Machida T, Takahashi S, et al. Fas-mediated apoptosome formation is dependent on reactive oxygen species derived from mitochondrial permeability transition in Jurkat cells. J Immunol **2004**; 173:285–96.
25. Kizhakkayil J, Thayyullathil F, Chathoth S, Hago A, Patel M, Galadari S. Glutathione regulates caspase-dependent ceramide production and curcumin-induced apoptosis in human leukemic cells. Free Radic Biol Med **2012**; 52:1854–64.
26. Komatsu N, Nakagawa M, Oda T, Muramatsu T. Depletion of intracellular NAD(+) and ATP levels during ricin-induced apoptosis through the specific ribosomal inactivation results in the cytolysis of U937 cells. J Biochem **2000**; 128:463–70.
27. Muldoon DF, Hassoun EA, Stohs SJ. Ricin-induced hepatic lipid peroxidation, glutathione depletion, and DNA single-strand breaks in mice. Toxicon **1992**; 30:977–84.
28. Benard O, Balasubramanian KA. Effect of enterotoxin on glutathione status in the intestinal mucosa. Indian J Biochem Biophys **1996**; 33:409–13.
29. Leyva-Illades D, Cherla RP, Galindo CL, Chopra AK, Tesh VL. Global transcriptional response of macrophage-like THP-1 cells to Shiga toxin type 1. Infect Immun **2010**; 78:2454–65.
30. Schmid DI, Kohan DE. Effect of shigatoxin-1 on arachidonic acid release by human glomerular epithelial cells. Kidney Int **2001**; 60:1026–36.

31. Zoja C, Casiraghi F, Morigi M. Shiga toxin modulates prostacyclin (PGI2) release in human renal microvascular endothelial cells (HRMEC). Presented at: Second International Symposium and Workshop on Verocytotoxin (Shiga-like toxin)–producing *Escherichia coli* Infections, Bergamo, Italy, **1994**:90.
32. Karch H, Bitzan M, Pietsch R. Purified verotoxins of *Escherichia coli* O157: H7 decrease prostacyclin synthesis by endothelial cells. Microb Pathog **1988**; 5:215–21.
33. Túri S, Beattie TJ, Belch JJ, Murphy AV. Disturbances of prostacyclin metabolism in children with hemolytic-uremic syndrome and in first degree relatives. Clin Nephrol **1986**; 25:193–8.
34. Stuart MJ, Spitzer RE, Walenga RW, Boone S. Prostanoids in hemolytic uremic syndrome. J Pediatr **1985**; 106:936–9.
35. Tönshoff B, Momper R, Kühl PG, Schweer H, Schärer K, Seyberth HW. Increased thromboxane biosynthesis in childhood hemolytic uremic syndrome. Kidney Int **1990**; 37:1134–41.
36. Noris M, Benigni A, Siegler R, et al. Renal prostacyclin biosynthesis is reduced in children with hemolytic-uremic syndrome in the context of systemic platelet activation. Am J Kidney Dis **1992**; 20:144–9.
37. Siegler R, Pysher T, Tesh V, Taylor F. Renal prostacyclin biosynthesis in a baboon model of Shiga toxin mediated hemolytic uremic syndrome. Nephron **2002**; 2204:363–8.
38. Bobbio-Pallavicini E, Porta C, Tacconi F, et al. Intravenous prostacyclin (as epoprostenol) infusion in thrombotic thrombocytopenic purpura. Four case reports and review of the literature. Italian Cooperative Group for Thrombotic Thrombocytopenic Purpura. Haematologica **1994**; 79:429–37.
39. Beattie TJ, Murphy AV, Willoughby ML, Belch JJ. Prostacyclin infusion in haemolytic-uraemic syndrome of children. Br Med J (Clin Res Ed) **1981**; 283:470.
40. Benigni A, Remuzzi G. The role of eicosanoids in the pathogenesis of hemolytic uremic syndrome. Prostaglandins Leukot Essent Fatty Acids **1994**; 51:75–9.
41. Taylor C, Lote C. Prostacyclin in diarrhoea-associated haemolytic uraemic syndrome. Pediatr Nephrol **1993**; 2012:416749.
42. Pawlak K, Myśliwiec M, Pawlak D. Kynurenine pathway - a new link between endothelial dysfunction and carotid atherosclerosis in chronic kidney disease patients. Adv Med Sci **2010**; 55:196–203.
43. Pawlak D, Tankiewicz A, Buczko W. Kynurenine and its metabolites in the rat with experimental renal insufficiency. J Physiol Pharmacol **2001**; 52(4 Pt 2):755–66.
44. Pawlak D, Pawlak K, Malyszko J, Mysliwiec M, Buczko W. Accumulation of toxic products degradation of kynurenine in hemodialyzed patients. Int Urol Nephrol **2001**; 33:399–404.
45. Krause R, Zollner-Schwetz I, Salzer HJF, et al. Elevated levels of interleukin 17A and kynurenine in candidemic patients, compared with levels in noncandidemic patients in the intensive care unit and those in healthy controls. J Infect Dis **2015**; 211:445–51.
46. Barth MC, Ahluwalia N, Anderson TJT, et al. Kynurenic acid triggers firm arrest of leukocytes to vascular endothelium under flow conditions. J Biol Chem **2009**; 284:19189–95.
47. van Setten PA, van Hinsbergh VW, van der Velden TJ, et al. Effects of TNF alpha on verocytotoxin cytotoxicity in purified human glomerular microvascular endothelial cells. Kidney Int **1997**; 51:1245–56.
48. Karsan A, Yee E, Kaushansky K, Harlan JM. Cloning of human Bcl-2 homologue: inflammatory cytokines induce human A1 in cultured endothelial cells. Blood **1996**; 87:3089–96.
49. López EL, Contrini MM, Devoto S, et al. Tumor necrosis factor concentrations in hemolytic uremic syndrome patients and children with bloody diarrhea in Argentina. Pediatr Infect Dis J **1995**; 14:594–8.
50. Pijpers AH, van Setten PA, van den Heuvel LP, et al. Verocytotoxin-induced apoptosis of human microvascular endothelial cells. J Am Soc Nephrol **2001**; 12:767–78.